

Hybrid Structures and Strain-Tunable Electronic Properties of Carbon Nanothreads

Weikang Wu,[†] Bo Tai,[†] Shan Guan,^{*,‡,†} Shengyuan A. Yang,^{*,†} and Gang Zhang^{*,¶}

[†]*Research Laboratory for Quantum Materials, Singapore University of Technology and Design, Singapore 487372, Singapore*

[‡]*Beijing Key Laboratory of Nanophotonics and Ultrafine Optoelectronic Systems, School of Physics, Beijing Institute of Technology, Beijing 100081, China.*

[¶]*Institute of High Performance Computing, Agency for Science, Technology and Research, 1 Fusionopolis Way, Singapore 138632, Singapore.*

E-mail: physguan@gmail.com; shengyuan_yang@sutd.edu.sg; zhangg@ihpc.a-star.edu.sg

Abstract

The newly synthesized ultrathin carbon nanothreads have drawn great attention from the carbon community. Here, based on first-principles calculations, we investigate the electronic properties of carbon nanothreads under the influence of two important factors: the Stone-Wales (SW) type defect and the lattice strain. The SW defect is intrinsic to the polymer-I structure of the nanothreads and is a building block for the general hybrid structures. We find that the bandgap of the nanothreads can be tuned by the concentration of SW defects in a wide range of $3.92 \sim 4.82$ eV, interpolating between the bandgaps of sp^3 -(3,0) structure and the polymer-I structure. Under strain, the bandgaps of all the structures, including the hybrid ones, show a nonmonotonic variation: the bandgap first increases with strain, then drops at large strain above 10%. The gap size can be effectively tuned by strain in a wide range (> 0.5 eV). Interestingly, for sp^3 -(3,0) structure, a switch of band ordering occurs under strain at the valence band maximum, and for the polymer-I structure, an indirect-to-direct-bandgap transition occurs at about 8% strain. The result also indicates that the presence of SW defects tends to stabilize the bandgap size against strain. Our findings suggest the great potential of structure- and strain-engineered carbon nanothreads in optoelectronic and photoelectrochemical applications as well as stress sensors.

Introduction

Carbon nanotubes have attracted tremendous interest, because of their extraordinarily small diameters, robust stability, and excellent electronic properties.¹⁻³ Remarkable observations have been made that the electronic properties of CNTs are sensitively determined by its chiral vector (n, m) and the diameter D ,⁴⁻⁹ including metallic tubes ($n = m$), small-gap semiconductors ($n - m = 3l$ with l an integer) with gap size $\propto 1/D^2$, and insulating tubes with large gaps proportional to $1/D$. The electronic properties of carbon nanotubes may be strongly modified by the structural defects, which are often inevitable during fabrication processes.¹⁰⁻¹³ Especially, one type of structural defects, the Stone-Wales (SW) defect,¹⁴ has been found to exhibit many interesting effects. The SW defect consists of a pentagon-heptagon pair, which is induced by a 90° rotation of a C-C bond in the hexagonal structures. Its presence can close the bandgap for large-gap nanotubes, open gaps for small-gap nanotubes, or increase the density of states for metallic ones.^{10,11} Choi *et al.* showed that SW defects can generate two quasi-bound states, leading to two quantized conductance reductions above and below the Fermi energy in metallic (10,10) nanotubes.^{15,16} Furthermore, it has been demonstrated experimentally that the presence of SW defects can be readily controlled by mechanical distortion or by electron irradiation.^{17,18} Thus, the SW defects provide an alternative route to engineer the electronic properties of carbon structures.

Continuing efforts have been devoted to achieving tubes with smaller diameters. The motivation is partly from the expectation that the small nanotubes may exhibit interesting electronic properties due to the strong σ^* and π^* orbital mixing.¹⁹ The challenge is that for very small diameters (below 1 nm), the large curvature distortion typically causes the bond angles in the structure far below the ideal 120° sp^2 angle, making the structure unstable. One possible solution is through attaching tightly-bonded groups (e.g., hydrogen or fluorine) to the structure, such that the sp^2 -hybridized tube can be converted to a more stable sp^3 -hybridized tube.²⁰ Recently, such an ultrathin sp^3 carbon nanomaterial, called the carbon nanothread, has been successfully synthesized through the high-pressure solid-state reac-

tion of benzene.²¹ Most recently, carbon nanothreads with long-range order over hundreds of microns have been demonstrated through a mechanochemical synthesis method.²² The word "nanothread" emphasizes its ultra-small diameter and the sp^3 -bonding character of its carbon atoms is similar to that of diamond. It represents an ideal one-dimensional (1D) material, and its diameter is only about 6.4 Å. Theoretically, many topologically distinct structures are predicted for the nanothreads.²³ Experimentally, from the derived pair distribution functions, the structure of carbon nanothreads were suggested to be a hybrid of two types of structures: the so-called sp^3 -(3,0) structure²⁰ and the polymer-I structure.²⁴ The sp^3 -(3,0) nanothread can be viewed as a fully hydrogenated (3,0) carbon nanotube, while the polymer-I nanothread can be regarded as a 1D chain of SW defects with hydrogenated carbon atoms. In fact, starting from a pure sp^3 -(3,0) nanothread, one can make a polymer-I nanothread by inserting the SW defects. The structures that interpolate between the two pristine types, i.e. nanothreads with sp^3 -(3,0) domains connected by SW defects, may be termed as SW hybrid structures. Excellent mechanical and thermal properties have been proposed for these carbon nanothreads.^{25–29} For example, hybrid nanothreads are predicted to have a high stiffness of about 665-850 GPa and a large specific strength of 3.97×10^7 to 4.1×10^7 N·m/kg, based on molecular dynamics (MD) simulations.²⁵ And the structures show a brittle to ductile transition when the concentration of SW defects increases.²⁶ Such properties make carbon nanothreads ideal for reinforced composites, strain sensors, and thermal connections.^{29,30}

Besides mechanical and thermal properties, the electronic properties of carbon nanothreads also begin to attract attention. Preliminary studies have shown that carbon nanothreads are electrical insulators similar to diamonds,²⁰ and their electronic properties can be tuned through chemical functionalization.³¹ In view of the important effects of SW defects as revealed in other carbon allotropes as well as the intrinsic presence of SW defects in polymer-I and hybrid nanothreads, it is of great interest to investigate how the SW defects modify the electronic properties of carbon nanothreads. Meanwhile, given the excellent mechanical

properties of carbon nanothreads, it is natural to expect that strain may provide a powerful tool for tuning the electronic properties, as evidenced in the studies of other low-dimensional materials.^{32–36} In this work, we investigate these two issues using first-principles calculations. We focus on the pristine sp^3 -(3,0) and polymer-I nanothreads and the SW hybrid nanothreads, which are the most relevant ones to experiment. We find that the bandgap of carbon nanothreads can be tuned by the SW defect concentration in a wide range as large as 1 eV, interpolating between the bandgaps of sp^3 -(3,0) and polymer-I nanothreads. Under strain, the bandgaps of the nanothreads, including both pristine nanothreads and hybrid nanothreads, show a nonmonotonic variation. The bandgap widens with strain by about 0.5 eV up to a critical strain then dramatically drops with further increasing strain. Interestingly, for the sp^3 -(3,0) nanothread, there is a switch of band ordering near the valence band maximum (VBM) with increasing strain; while for the polymer-I nanothread, there is an indirect-to-direct-bandgap transition occurring at about 8% strain. Our work reveals that SW defects and strain offer powerful tools to control the electronic properties of carbon nanothreads, making them a promising platform for optoelectronic and photoelectrochemical applications.

Computational Methods

The first-principles calculations were performed based on the density functional theory (DFT) using the projector augmented wave method³⁷ as implemented in the Vienna *ab initio* simulation package.^{38,39} The generalized gradient approximation (GGA) with the Perdew-Burke-Ernzerhof (PBE) realization was adopted for the exchange-correlation potential.⁴⁰ $1s^1$ and $2s^22p^2$ were treated as the valence orbitals for H and C, respectively. The cutoff energy for the plane-wave basis was set to 500 eV, and the energy convergence criterion is set to be 10^{-5} eV. The cell parameters and the ionic positions are fully optimized until the residual force on each atom is less than 10^{-2} eV/Å. For pristine sp^3 -(3,0) and polymer-I nanothreads, a cubic cell of size $15 \text{ Å} \times 15 \text{ Å} \times c \text{ Å}$ was used, which is large enough to eliminate the artificial

interactions between the periodic images. To investigate the SW hybrid structures, $1 \times 1 \times 4$ supercells (with size $15 \text{ \AA} \times 15 \text{ \AA} \times 4c \text{ \AA}$) were employed to realize hybrid structures with different SW defect concentrations. The Brillouin zone was sampled with the Γ -centered k mesh of sizes $1 \times 1 \times 11$ for the cubic cell, and $1 \times 1 \times 4$ for the supercell, respectively. Under strain, the atomic positions are fully relaxed without any constraint. To calculate the virial stress under strain, the cross-sectional area of the structure is approximated by λV_0 , where λ is the linear atom density (shown in Table 1) and V_0 is a reference atomic volume for carbon atom in bulk diamond, which is about $5.536 \text{ \AA}^3/\text{atom}$. The same approach was previously used to characterize the (3,0) and (2,2) sp^3 tubes.²⁰ It should be noted that different approaches for calculating the cross-sectional area would yield different absolute values of the stress, but it will not affect the scaling behaviours as we focus on in this paper.

Results and Discussion

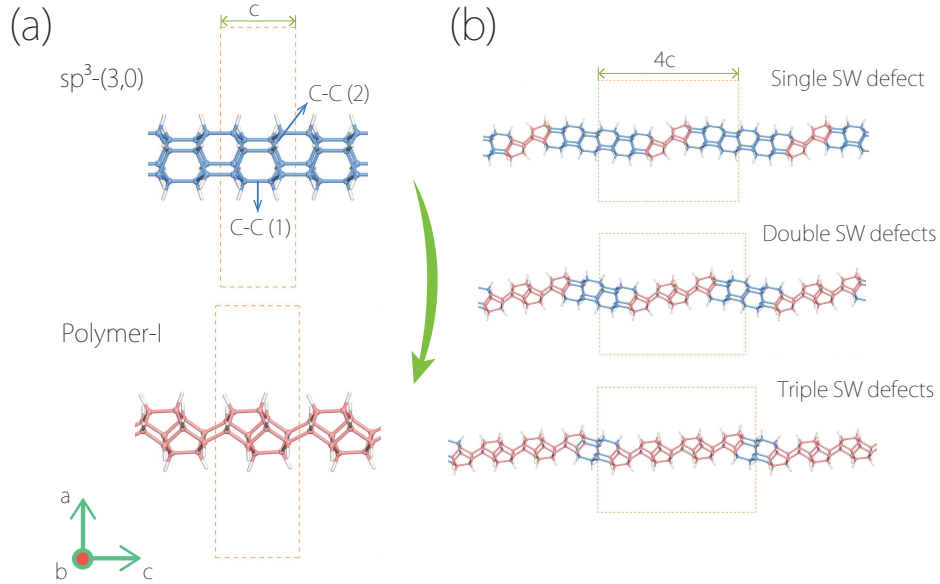


Figure 1: Structures of carbon nanothreads. (a) Structures of sp^3 -(3,0) nanothread (upper panel) and polymer-I nanothread (lower panel). The C-C (1) and C-C (2) label the two types of C-C bonds in the sp^3 -(3,0) nanothread. (b) SW hybrid nanothreads with single, double, and triple SW defects in a supercell. In the modelling, $1 \times 1 \times 4$ supercells are employed. Here the red color marks the SW defect regions.

The carbon nanothread models were constructed based on the recent experimental observations as well as first-principles calculations.^{21,23} The two pristine structures, the sp^3 -(3,0) and the polymer-I structures, are shown in Fig. 1(a). One observes that the sp^3 -(3,0) nanothread can be viewed as a fully hydrogenated (3,0) carbon nanotube without a SW defect, whereas the polymer-I nanothread can be regarded as a chain of SW defects. In the sp^3 -(3,0) structure, there are two types of C-C bonds, C-C (1) and C-C (2) [see Fig.1(a)], with the bond lengths of 1.569 Å and 1.544 Å, respectively. And the average C-C bond length for the polymer-I structure is about 1.550 Å. These values are in good agreement with the experimental data (~ 1.52 Å).²¹ By generating SW defects in the sp^3 -(3,0) structure, one can make the SW hybrid structures [see Fig. 1(b)] that interpolate between the two pristine structures. In this work, we adopt a $1 \times 1 \times 4$ supercell, so the number of SW defects in a single supercell ranges from 1 to 3, as shown in Fig. 1(b). Each SW hybrid nanothread consists of two distinct sections: the sp^3 -(3,0) domain and the SW defect domain.

Table 1: The linear carbon atom density λ , energy per $(CH)_6$ unit, and bandgap for the SW hybrid nanothreads. The energies are relative to a single sheet of graphane.

	$\lambda = N/c$ (C atom/Å)	Energy (eV/ $(CH)_6$)	Bandgap (eV)
sp^3 -(3,0)	2.792	0.710	3.92
single SW	2.733	0.719	4.07
double SW	2.637	0.737	4.22
triple SW	2.525	0.759	4.53
Polymer-I	2.410	0.795	4.82

From our calculation, we find that the SW defects tend to stretch the length of the nanothreads, which can also be observed by the decreasing linear carbon atom density (λ) with the increasing number of SW defects (see Table 1). For the sp^3 -(3,0) nanothread, $\lambda = 2.792$ atoms/Å, in accordance with the previous theoretical work.²³ And the polymer-I nanothread exhibits the lowest linear density. As the concentration of SW defects increases from 0% to 100%, the energy per $(CH)_6$ unit exhibits a continuing increase, similar to the previous MD simulation result which shows that adding a SW defect would increase the

potential energy of carbon nanothreads.²⁵

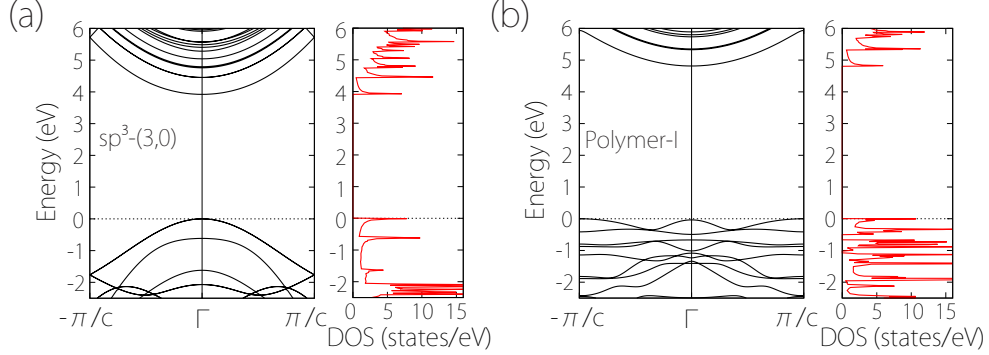


Figure 2: Band structures along with density of states (DOS) for (a) sp^3 -(3,0) nanothread and (b) polymer-I nanothread. The Fermi level is set at valence band maximum (VBM).

The calculated band structures of sp^3 -(3,0) and polymer-I nanothreads along with the density of states (DOS) are shown in Fig. 2. Due to the sp^3 C-C bonding with saturated hydrocarbons, both nanothreads are wide-bandgap semiconductors, with gap value exceeding those obtained in sp^2 carbon nanotubes.⁷ The sp^3 -(3,0) nanothread has a direct bandgap of about 3.92 eV at the Γ point, whereas the polymer-I nanothread has an indirect bandgap with a larger value of 4.82 eV, close to the bandgap values in the previous theoretical work.²³ For the polymer-I nanothread, the conduction band minimum (CBM) is at the Γ point, but the VBM is located at the Brillouin zone boundary. Comparing with the VBM in sp^3 -(3,0) nanothreads, the much flatter bands near the VBM in the polymer-I nanothread show much larger hole effective mass and a more localized character. This feature is also reflected in the DOS for the two structures: One clearly observes that the DOS for polymer-I has a more pronounced peak near VBM in comparison with that for sp^3 -(3,0).

When SW defects are introduced into the sp^3 -(3,0) nanothread, the bandgap widens as shown in Table 1. The value increases from 4.07 eV for the hybrid structure with one SW defect up to 4.82 eV for the polymer-I nanothread which is fully composed of SW defects. This indicates that SW defects can be used to control the bandgaps of carbon nanothreads. In Fig. 3, we plot the band structures of the SW hybrid nanothreads. As shown in Fig. 3(a), for the structure with one SW defect in a supercell, a quite flat band

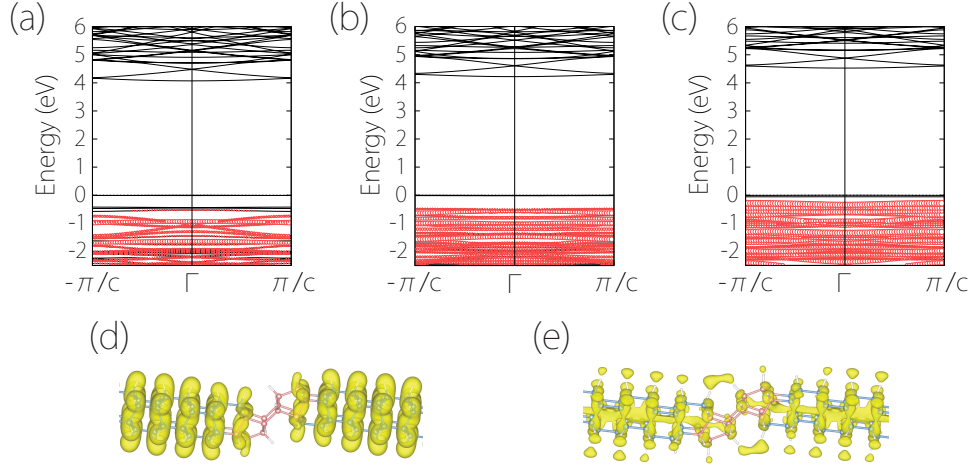


Figure 3: Band structures of SW hybrid nanothreads with (a) single SW defect, (b) double SW defects, and (c) triple SW defects. The Fermi level is set at VBM. The size of the red circles in (a-c) indicates the weight of projection onto the C atoms in the SW defect domains. (d,e) Charge density contour plots for (d) VBM and (e) CBM at the Γ point around a single SW defect.

appears above the original VBM. We analyze the charge density distribution for states of this flat band [see Fig. 3(d)], and find that the flat band mainly involves states distributed in the sp^3 -(3,0) domains, not on the SW defects. Instead, the states distributed on the SW defects contribute to the states below the VBM. This observation implies that the presence of SW defects tend to localize the valence band states in the sp^3 -(3,0) domains. The charge distribution of the CBM state is plotted in Fig. 3(e), from which one observes that the state is mainly distributed inside the thread. The continuous charge distribution is suppressed at the SW defect region. As a result of this enhanced confinement, the presence of defect tends to push up the CBM state in energy, as observed in Fig. 3(a-c). For comparison, in the previous study on sp^2 (8,0) and (14,0) carbon nanotubes, SW defects are found to enlarge the bandgap size through inducing the localized electronic states in the bandgap, but the gap size decreases with increasing defect concentration.⁴¹

Next, we study the strain effects on the electronic properties of carbon nanothreads. Since low-dimensional materials are prone to wrinkle under lateral compression, here we

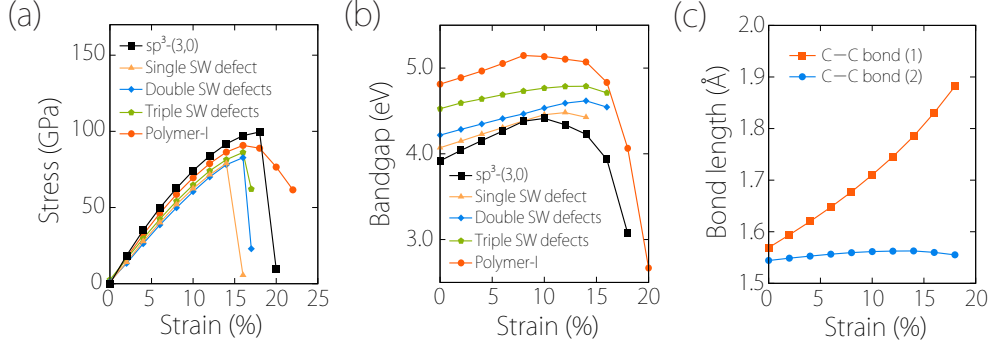


Figure 4: (a) Strain-stress relations and (b) bandgap versus strain curves for the different types of carbon nanotubes. (c) The bond-lengths versus strain for the sp^3 -(3,0) nanothread.

focus on the tensile strain. The strain is defined as $\varepsilon = (l - l_0)/l_0 \times 100\%$, where l and l_0 are the lengths of strained and unstrained structures, respectively. Figure 4(a) shows the strain-stress relations of the different types of nanotreads. We find that the sp^3 -(3,0) nanothread and hybrid nanotreads exhibit brittle behaviour with the failure strain below $\sim 20\%$, whereas the polymer-I nanothread can sustain up to $\sim 22\%$ strain in accordance with the previous work.²⁷

Strain effectively tunes the bandgaps of the nanotreads. From Fig. 4(b), all nanotreads show a trend of increasing bandgap as the strain increases from zero, but the bandgap drops at larger strain. For the sp^3 -(3,0) nanothread, under strain, the bandgap increases from 3.92 eV to the maximum of 4.41 eV at $\varepsilon = 10\%$, while the polymer-I nanothread shows a maximum bandgap of 5.15 eV at the strain of 8%. Notably, for a fixed strain, the bandgap value still increases with the concentration of SW defects. As the number of SW defects increases, the increasing trend of bandgap can be sustained to larger strains, and the slope of bandgap versus strain curve decreases. This shows that the presence of SW defects tends to stabilize the bandgap size against strain.

To further investigate the effects of strain on the electronic properties, we plot the band structures of sp^3 -(3,0) and polymer-I nanotreads under several different strains in Figs. 5(a) and 5(b). One observes that the CBMs of both sp^3 -(3,0) and polymer-I nanotreads remain almost unchanged. The main change occurs at the VBM. For the sp^3 -(3,0) nanothread,

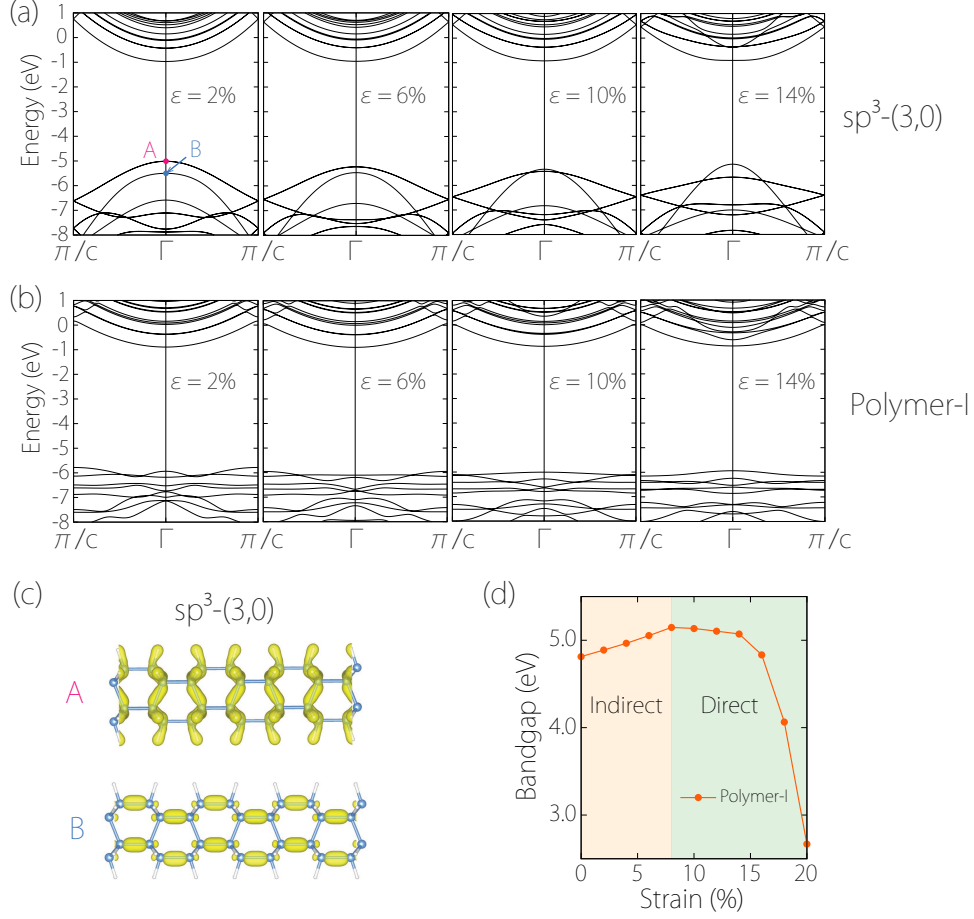


Figure 5: Band structures of (a) sp^3 -(3,0) nanothread and (b) polymer-I nanothread under the strains of 2%, 6%, 10%, and 14%. All energies are referenced to the vacuum level. The charge density contour plots of A and B states (as indicated in (a)) at the Γ point for the sp^3 -(3,0) nanothread. (d) Indirect-to-direct-bandgap transition in polymer-I nanothread.

there is an interesting band switching between two bands near VBM at about 8% strain. As indicated in Figs. 5(a), the original VBM state A is shifted down in energy, causing the increase of bandgap before $\varepsilon = 8\%$. Meanwhile, the B state, initially below A state by ~ 0.5 eV, is shifted up in energy with increasing strain, and at $\varepsilon \approx 8\%$, it crosses the A state and becomes the new VBM. After the band switching, the B state keeps moving up in energy, leading to the decrease of bandgap. This picture explains the nonmonotonic variation of bandgap value as observed in Fig. 4(b).

The different responses of A and B states to strain can be understood from their bonding characters. From the charge distribution of the two states plotted in Fig. 5(c), one observes

that the A state has an antibonding character between the adjacent benzenes, whereas the B state exhibits a bonding character. From Fig. 4(c), the C-C bond (1) shows continuous increase in length under strain. Hence under strain, A state is pulled down whereas the B state is pushed up in energy, which produces the band switching phenomenon. This band switching could lead to dramatic changes in the electronic properties. For example, here the band with A state is flatter than the band with B state. Hence for the case with hole doping, the effective mass of the hole carriers should have a sudden drop when the strain is increased across the critical strain for band switching.

Similar band switching phenomenon also happens in the polymer-I nanothread between $\varepsilon = 2\%$ and 6% for the two bands at the Γ point [see Fig. 5(b)]. However, the unstrained polymer-I is an indirect bandgap semiconductor with the CBM at Γ point and the VBM at $k = \pm\pi/c$. The band switching does not affect the location of VBM. Interestingly, with further increasing strain above 8% , the valence band state at the Γ point rises above the state at the $k = \pm\pi/c$ point and becomes the new VBM. This causes an indirect-to-direct-bandgap transition induced by strain [see Fig. 5(d)]. The character of direct/indirect gap is important in determining optical properties of a semiconductor. For example, the intensity of photoluminescence will be much stronger for a direct-gap semiconductor compared with an indirect-gap one. Hence, it is possible to effectively control the optical properties of polymer-I nanothreads by strain.

Conclusion

Based on first-principles calculations, we have revealed the interesting effects of SW defects and lattice strain on the electronic properties of the newly synthesized carbon nanothreads. The bandgap of nanothreads can be tuned within a wide range of ~ 1 eV by the SW defects in the hybrid structures, interpolating between the bandgaps of sp^3 -(3,0) and polymer-I nanothreads. Under applied strain, the bandgaps of nanothreads show a nonmonotonic

variation. The bandgap value first increases with strain, then drops at large strain above 10%. The gap size can be effectively tuned by strain in a wide range above > 0.5 eV. Interestingly, for the sp^3 -(3,0) nanothread, a switch of band ordering occurs under strain at the valence band maximum, which can dramatically affect the properties of hole carriers, and for the polymer-I nanothread, an indirect-to-direct-bandgap transition occurs at about 8% strain, which is expected to strongly affect its optical properties. Since the wide-bandgap diamond has been demonstrated to be a very promising deep-ultraviolet photodetector with solar blindness,⁴² given that the carbon nanothreads are of similar bandgap size, they would also offer an encouraging opportunity for applications as photodetectors. Our work suggests that the SW defects and strain offer powerful tools to engineer the properties of carbon nanothreads for future optoelectronic and photoelectrochemical applications as well as stress sensors.

Acknowledgement

This work is supported by Singapore MOE Academic Research Fund Tier 1 (SUTD-T1-2015004). ZG gratefully acknowledges the financial support from the Agency for Science, Technology and Research (A*STAR), Singapore and the use of computing resources at the A*STAR Computational Resource Centre, Singapore. We also acknowledge the computational support from National Supercomputing Centre Singapore and the Texas Advanced Computing Center.

References

- (1) Tans, S. J.; Verschueren, A. R.; Dekker, C. Room-Temperature Transistor Based on a Single Carbon Nanotube. *Nature* **1998**, *393*, 49–52.

- (2) De Volder, M. F.; Tawfick, S. H.; Baughman, R. H.; Hart, A. J. Carbon Nanotubes: Present and Future Commercial Applications. *Science* **2013**, *339*, 535–539.
- (3) Avouris, P. Molecular Electronics with Carbon Nanotubes. *Acc. Chem. Res.* **2002**, *35*, 1026–1034.
- (4) Kane, C. L.; Mele, E. Size, Shape, and Low Energy Electronic Structure of Carbon Nanotubes. *Phys. Rev. Lett.* **1997**, *78*, 1932–1935.
- (5) Ouyang, M.; Huang, J.-L.; Cheung, C. L.; Lieber, C. M. Energy Gaps in "Metallic" Single-Walled Carbon Nanotubes. *Science* **2001**, *292*, 702–705.
- (6) White, C.; Mintmire, J. Density of States Reflects Diameter in Nanotubes. *Nature* **1998**, *394*, 29–30.
- (7) Hamada, N.; Sawada, S.-i.; Oshiyama, A. New One-Dimensional Conductors: Graphitic Microtubules. *Phys. Rev. Lett.* **1992**, *68*, 1579–1581.
- (8) Saito, R.; Fujita, M.; Dresselhaus, G.; Dresselhaus, u. M. Electronic Structure of Chiral Graphene Tubules. *Appl. Phys. Lett.* **1992**, *60*, 2204–2206.
- (9) Charlier, J.-C.; Blase, X.; Roche, S. Electronic and Transport Properties of Nanotubes. *Rev. Mod. Phys.* **2007**, *79*, 677–732.
- (10) Crespi, V. H.; Cohen, M. L.; Rubio, A. In Situ Band Gap Engineering of Carbon Nanotubes. *Phys. Rev. Lett.* **1997**, *79*, 2093–2096.
- (11) Andriotis, A. N.; Menon, M.; Srivastava, D. Transfer Matrix Approach to Quantum Conductivity Calculations in Single-Wall Carbon Nanotubes. *J. Chem. Phys.* **2002**, *117*, 2836–2843.
- (12) He, Y.; Zhang, C.; Cao, C.; Cheng, H.-P. Effects of Strain and Defects on the Electron Conductance of Metallic Carbon Nanotubes. *Phys. Rev. B* **2007**, *75*, 235429.

- (13) Collins, P. G.; Bradley, K.; Ishigami, M.; Zettl, A. Extreme Oxygen Sensitivity of Electronic Properties of Carbon Nanotubes. *Science* **2000**, *287*, 1801–1804.
- (14) Stone, A. J.; Wales, D. J. Theoretical Studies of Icosahedral C₆₀ and Some Related Species. *Chem. Phys. Lett.* **1986**, *128*, 501–503.
- (15) Choi, H. J.; Ihm, J. Ab Initio Pseudopotential Method for the Calculation of Conductance in Quantum Wires. *Phys. Rev. B* **1999**, *59*, 2267–2275.
- (16) Choi, H. J.; Ihm, J.; Louie, S. G.; Cohen, M. L. Defects, Quasibound States, and Quantum Conductance in Metallic Carbon Nanotubes. *Phys. Rev. Lett.* **2000**, *84*, 2917–2920.
- (17) Nardelli, M. B.; Yakobson, B. I.; Bernholc, J. Mechanism of Strain Release in Carbon Nanotubes. *Phys. Rev. B* **1998**, *57*, R4277–R4280.
- (18) Kotakoski, J.; Meyer, J.; Kurasch, S.; Santos-Cottin, D.; Kaiser, U.; Krasheninnikov, A. Stone-Wales-Type Transformations in Carbon Nanostructures Driven by Electron Irradiation. *Phys. Rev. B* **2011**, *83*, 245420.
- (19) Blase, X.; Benedict, L. X.; Shirley, E. L.; Louie, S. G. Hybridization Effects and Metallicity in Small Radius Carbon Nanotubes. *Phys. Rev. Lett.* **1994**, *72*, 1878–1881.
- (20) Stojkovic, D.; Zhang, P.; Crespi, V. H. Smallest Nanotube: Breaking the Symmetry of sp³ Bonds in Tubular Geometries. *Phys. Rev. Lett.* **2001**, *87*, 125502.
- (21) Fitzgibbons, T. C.; Guthrie, M.; Xu, E.-s.; Crespi, V. H.; Davidowski, S. K.; Cody, G. D.; Alem, N.; Badding, J. V. Benzene-Derived Carbon Nanothreads. *Nat. Mater.* **2015**, *14*, 43–47.
- (22) Li, X.; Baldini, M.; Wang, T.; Chen, B.; Xu, E.-s.; Vermilyea, B.; Crespi, V. H.; Hoffmann, R.; Molaison, J. J.; Tulk, C. A. et al. Mechanochemical Synthesis of Carbon Nanothread Single Crystals. *J. Am. Chem. Soc.* **2017**, *139*, 16343–16349.

- (23) Xu, E.-s.; Lammert, P. E.; Crespi, V. H. Systematic Enumeration of sp^3 Nanothreads. *Nano Lett.* **2015**, *15*, 5124–5130.
- (24) Wen, X.-D.; Hoffmann, R.; Ashcroft, N. Benzene under High Pressure: A Story of Molecular Crystals Transforming to Saturated Networks, with a Possible Intermediate Metallic Phase. *J. Am. Chem. Soc.* **2011**, *133*, 9023–9035.
- (25) Roman, R. E.; Kwan, K.; Cranford, S. W. Mechanical Properties and Defect Sensitivity of Diamond Nanothreads. *Nano Lett.* **2015**, *15*, 1585–1590.
- (26) Zhan, H.; Zhang, G.; Tan, V. B.; Cheng, Y.; Bell, J. M.; Zhang, Y.-W.; Gu, Y. From Brittle to Ductile: A Structure Dependent Ductility of Diamond Nanothread. *Nanoscale* **2016**, *8*, 11177–11184.
- (27) Silveira, J. F.; Muniz, A. R. First-Principles Calculation of the Mechanical Properties of Diamond Nanothreads. *Carbon* **2017**, *113*, 260–265.
- (28) Zhan, H.; Zhang, G.; Bell, J. M.; Gu, Y. The Morphology and Temperature Dependent Tensile Properties of Diamond Nanothreads. *Carbon* **2016**, *107*, 304–309.
- (29) Zhan, H.; Zhang, G.; Zhang, Y.; Tan, V.; Bell, J. M.; Gu, Y. Thermal Conductivity of a New Carbon Nanotube Analog: The Diamond Nanothread. *Carbon* **2016**, *98*, 232–237.
- (30) Zhan, H.; Zhang, G.; Tan, V. B.; Gu, Y. The Best Features of Diamond Nanothread for Nanofibre Applications. *Nat. Commun.* **2017**, *8*, 14863.
- (31) Silveira, J.; Muniz, A. Functionalized Diamond Nanothreads from Benzene Derivatives. *Phys. Chem. Chem. Phys.* **2017**, *19*, 7132–7137.
- (32) Minot, E.; Yaish, Y.; Sazonova, V.; Park, J.-Y.; Brink, M.; McEuen, P. L. Tuning Carbon Nanotube Band Gaps with Strain. *Phys. Rev. Lett.* **2003**, *90*, 156401.

- (33) Levy, N.; Burke, S.; Meaker, K.; Panlasigui, M.; Zettl, A.; Guinea, F.; Neto, A. C.; Crommie, M. Strain-Induced Pseudo-Magnetic Fields Greater than 300 Tesla in Graphene Nanobubbles. *Science* **2010**, *329*, 544–547.
- (34) Guinea, F.; Katsnelson, M.; Geim, A. Energy Gaps and a Zero-Field Quantum Hall Effect in Graphene by Strain Engineering. *Nat. Phys.* **2010**, *6*, 30–33.
- (35) Guan, S.; Cheng, Y.; Liu, C.; Han, J.; Lu, Y.; Yang, S. A.; Yao, Y. Effects of Strain on Electronic and Optic Properties of Holey Two-Dimensional C₂N Crystals. *Appl. Phys. Lett.* **2015**, *107*, 231904.
- (36) Wang, Y.; Wang, S.-S.; Lu, Y.; Jiang, J.; Yang, S. A. Strain-Induced Isostructural and Magnetic Phase Transitions in Monolayer MoN₂. *Nano Lett.* **2016**, *16*, 4576–4582.
- (37) Blöchl, P. E. Projector Augmented-Wave Method. *Phys. Rev. B* **1994**, *50*, 17953–17979.
- (38) Kresse, G.; Hafner, J. Ab Initio Molecular Dynamics for Liquid Metals. *Phys. Rev. B* **1993**, *47*, 558–561.
- (39) Kresse, G.; Furthmüller, J. Efficient Iterative Schemes for Ab Initio Total-Energy Calculations Using a Plane-Wave Basis Set. *Phys. Rev. B* **1996**, *54*, 11169–11186.
- (40) Perdew, J. P.; Burke, K.; Ernzerhof, M. Generalized Gradient Approximation Made Simple. *Phys. Rev. Lett.* **1996**, *77*, 3865–3868.
- (41) Zhou, Q.-X.; Wang, C.-Y.; Fu, Z.-B.; Tang, Y.-J.; Zhang, H. Effects of Various Defects on the Electronic Properties of Single-Walled Carbon Nanotubes: A First Principle Study. *Front. Phys.* **2014**, *9*, 200–209.
- (42) Liao, M.; Koide, Y.; Sang, L. Nanostructured Wide-Bandgap Semiconductors for Ultraviolet Detection. *Austin J. Nanomed. Nanotechnol.* **2014**, *2*, 1029.

Graphical TOC Entry

